# Renormalized quasiparticles in antiferromagnetic states of the Hubbard model

J. Bauer and A.C. Hewson

*Department of Mathematics, Imperial College, London SW7 2AZ, United Kingdom*

(Dated: January 25, 2014)

We analyze the properties of the quasiparticle excitations of metallic antiferromagnetic states in a strongly correlated electron system. The study is based on dynamical mean field theory (DMFT) for the infinite dimensional Hubbard model with antiferromagnetic symmetry breaking. Self-consistent solutions of the DMFT equations are calculated using the numerical renormalization group (NRG). The low energy behavior in these results is then analyzed in terms of renormalized quasiparticles. The parameters for these quasiparticles are calculated directly from the NRG derived self-energy, and also from the low energy fixed point of the effective impurity. They are found to be in good agreement. We show that the main low energy features of the $k$-resolved spectral density can be understood in terms of the quasiparticle picture. We also find that Luttinger's theorem is satisfied for the total electron number in the doped antiferromagnetic state.

## I. INTRODUCTION

The nature of the metallic antiferromagnetically ordered state in strongly correlated systems has been subject of study for over two decades, but still remains to be fully understood. Interest in this topic has been stimulated by the fact that the high temperature superconductivity of the cuprates emerges from the doping of an antiferromagnetic insulating compound, such as $La_2CuO_4$.[1,2] The simplest models to describe the electrons in the $CuO_2$ planes of the cuprates are the two dimensional $t$-$J$-model and Hubbard model. Much of the initial effort went into the study of a single hole state of these models in an antiferromagnetic background. For the motion of this hole, there is a competition between the gain in kinetic energy from the hopping and its disruptive effect on the antiferromagnetic order, and consequent loss of potential energy. As a result a hole excitation becomes a quasiparticle or magnetic polaron, heavily dressed by antiferromagnetic spin fluctuations (see review article by Dagotto[3] and references therein). Much of this work, however, relied on exact diagonalization or quantum Monte Carlo methods, which are limited to small clusters and very few hole excitations, and cannot be readily extended to study the many-hole, finite doping situation.

More recent studies capable of describing finite doping have concentrated on the relation between the antiferromagnetic fluctuations and superconducting order (for a review see[4] and the references therein). One of the main motivations is to understand whether the exchange of these types of fluctuations can provide a purely electronic mechanism for inducing superconductivity. Here, in this paper, we focus on the metallic antiferromagnetism, the doped state with long range antiferromagnetic order. Our interest is to examine how well the low energy excitations in this ordered state can be described in terms renormalized quasiparticles. To tackle this problem we use the infinite dimensional Hubbard model.

The simplification in the infinite dimensional limit is that the electron self-energy becomes local in character, with no wavevector dependence.[5,6] The self-energy then depends only on the frequency, as is the case for impurity models, allowing the lattice problem to be cast in the form of a self-consistent impurity model. There are several reasonably accurate techniques for solving this effective impurity problem, the most accurate for the zero and low temperature regime being the numerical renormalization group approach (NRG)[7].

Recently we studied the effect of a magnetic field on the quasiparticle excitations in the strong correlation regime of the infinite dimensional Hubbard model using the NRG method[8]. We also extended a form of renormalized perturbation theory (RPT), originally developed for impurity models[9], to this model, and used it to calculate the local dynamic spin susceptibilities, obtaining results in good overall agreement with those from the NRG. In this paper we extend this combination of renormalization techniques, NRG and RPT within dynamical mean field theory, to look at the low energy excitations of the infinite dimensional Hubbard model in a staggered field, and in antiferromagnetic broken symmetry states. Extensive calculations of the antiferromagnetic states in the Hubbard model using the DMFT-NRG approach have already been reported in the paper of Zitzler, Pruschke and Bulla[10]. We confirm their results for the phase diagram and extend the calculations and analysis to the description of the low energy renormalized excitations, and how these can be described within the framework of a renormalized perturbation theory.

## II. ANTIFERROMAGNETIC BROKEN SYMMETRY IN DMFT

In considering the response of the Hubbard model[11] to a staggered magnetic field and antiferromagnetic order, we take the case of a bipartite lattice, which consists of two sublattices $A$ and $B$ such that the nearest neighbors of a site in the $A$ sublattice are on the $B$ sublattice and

vice versa. The Hamiltonian for the Hubbard model can be written in the form,

$$H_\mu = \sum_{i,j,\sigma}(t_{ij}c^\dagger_{A,i,\sigma}c_{B,j,\sigma} + \text{h.c.}) + U\sum_{i,\alpha}n_{\alpha,i,\uparrow}n_{\alpha,i,\downarrow}$$
$$- \sum_{i,\sigma}(\mu_\sigma c^\dagger_{A,i,\sigma}c_{A,i,\sigma} + \mu_{-\sigma}c^\dagger_{B,i,\sigma}c_{B,i,\sigma}), \quad (1)$$

where the hopping matrix element is taken as $t_{ij} = -t$ between nearest sites $i$ and $j$ only, and zero otherwise, and $\alpha = A, B$. A staggered field $H^i_s$

$$H^i_s = \begin{cases} H & \text{for } i \in A \text{ sublattice} \\ -H & \text{for } i \in B \text{ sublattice} \end{cases} \quad (2)$$

has been included so that $\mu_\sigma = \mu + \sigma h$, where $h = g\mu_B H/2$ with the Bohr magneton $\mu_B$. The non-interacting part of the Hamiltonian $H_{0,\mu}$ can be diagonalized in terms of Bloch states and then expressed in the form,

$$H_{0,\mu} = \sum_{\boldsymbol{k},\sigma} C^\dagger_{\boldsymbol{k},\sigma}M_{\boldsymbol{k},\sigma}C_{\boldsymbol{k},\sigma}. \quad (3)$$

where $C^\dagger_{\boldsymbol{k},\sigma} = (c^\dagger_{A,\boldsymbol{k},\sigma}, c^\dagger_{B,\boldsymbol{k},\sigma})$, and the matrix $M_{\boldsymbol{k},\sigma}$ is given by

$$M_{\boldsymbol{k},\sigma} = \begin{pmatrix} -\mu_\sigma & \varepsilon_{\boldsymbol{k}} \\ \varepsilon_{\boldsymbol{k}} & -\mu_{-\sigma} \end{pmatrix}. \quad (4)$$

The $\boldsymbol{k}$ sums run over a reduced Brillouin zone, and the energy of the Bloch state is $\varepsilon_{\boldsymbol{k}} = \sum_j t_{ij}e^{i(\boldsymbol{R}_i-\boldsymbol{R}_j)\cdot\boldsymbol{k}}$. The free Green's function matrix $\underline{G}^0_{\boldsymbol{k},\sigma}(\omega)$ is given by $(\omega - M_{\boldsymbol{k},\sigma})^{-1}$. The poles of the free Green's function give the elementary single particle excitations, which are given by

$$E^0_{\boldsymbol{k},\pm}(U=0) = -\mu_0(h) \pm \sqrt{h^2 + \varepsilon^2_{\boldsymbol{k}}}, \quad (5)$$

where $\mu_0(h)$ is the chemical potential of the noninteracting system in a staggered field. This illustrates that the electronic excitations are split into two subbands for a finite staggered field.

Notice that we have adopted a special choice of basis $\{c_{A,\boldsymbol{k},\sigma}, c_{B,\boldsymbol{k},\sigma}\}$ here[10,12]. Another common basis to study antiferromagnetic and spin density wave symmetry (SDW) breaking is $\{c_{\boldsymbol{k},\sigma}, c_{\boldsymbol{k}+\boldsymbol{q}_0,\sigma}\}$, where $\boldsymbol{q}_0$ is the reciprocal lattice vector for commensurate SDW ordering. The bases can be related by a linear transformation,

$$\begin{pmatrix} c_{\boldsymbol{k},\sigma} \\ c_{\boldsymbol{k}+\boldsymbol{q}_0,\sigma} \end{pmatrix} = \frac{1}{\sqrt{2}}\begin{pmatrix} 1 & -1 \\ 1 & 1 \end{pmatrix}\begin{pmatrix} c_{A,\boldsymbol{k},\sigma} \\ c_{B,\boldsymbol{k},\sigma} \end{pmatrix}. \quad (6)$$

For the latter basis the matrix $M_{\boldsymbol{k},\sigma}$ would be diagonal in the kinetic energy term and the symmetry breaking is offdiagonal. For our study in the DMFT framework the $A-B$-sublattice basis is, however, more convenient and we will use it throughout the rest of this paper. It is possible, of course, to relate the obtained quantities with the help of (6) to the $\{c_{\boldsymbol{k},\sigma}, c_{\boldsymbol{k}+\boldsymbol{q}_0,\sigma}\}$ basis.

We can generalize the equations to the interacting problem by introducing a self-energy $\Sigma_{\alpha,\boldsymbol{k},\sigma}(\omega)$, so that the matrix Green's function can be written in the form

$$\underline{G}_{\boldsymbol{k},\sigma}(\omega) = \frac{1}{\zeta_{A,\boldsymbol{k},\sigma}(\omega)\zeta_{B,\boldsymbol{k},\sigma}(\omega) - \varepsilon^2_{\boldsymbol{k}}}\begin{pmatrix} \zeta_{B,\boldsymbol{k},\sigma}(\omega) & -\varepsilon_{\boldsymbol{k}} \\ -\varepsilon_{\boldsymbol{k}} & \zeta_{A,\boldsymbol{k},\sigma}(\omega) \end{pmatrix}, \quad (7)$$

where $\zeta_{\alpha,\boldsymbol{k},\sigma}(\omega) = \omega + \mu_\sigma - \Sigma_{\alpha,\boldsymbol{k},\sigma}(\omega)$. As we are dealing with the infinite dimensional limit of the model, we take the self-energy to be local so we can drop the $\boldsymbol{k}$ index. This is the reason why the self-energy has a single site index $\alpha = A, B$ and no offdiagonal terms appear in equation (7). The symmetry of the bipartite lattice gives $\Sigma_{B,\sigma}(\omega) = \Sigma_{A,-\sigma}(\omega) \equiv \Sigma_{-\sigma}(\omega)$ and hence

$$\zeta_{B,-\sigma}(\omega) = \zeta_{A,\sigma}(\omega) \equiv \zeta_\sigma(\omega),$$

where we have simplified the notation. To determine these quantities $\Sigma_\sigma(\omega)$ it is sufficient to focus on the $A$ sublattice only.

Summing the first component in the Green's function in equation (7) over $\boldsymbol{k}$ we obtain the Green's function for a site on the $A$ sublattice, $G^{\text{loc}}_\sigma(\omega)$,

$$G^{\text{loc}}_\sigma(\omega) = \frac{\zeta_{-\sigma}(\omega)}{\sqrt{\zeta_\sigma(\omega)\zeta_{-\sigma}(\omega)}}\int d\varepsilon \frac{\rho_0(\varepsilon)}{\sqrt{\zeta_\sigma(\omega)\zeta_{-\sigma}(\omega)} - \varepsilon}, \quad (8)$$

where $\rho_0(\varepsilon)$ is the density of states of the non-interacting system in the absence of the staggered field.

In the DMFT this local Green's function, and the self-energy $\Sigma_\sigma(\omega)$, are identified with the corresponding quantities for an effective impurity model[12]. This implies that the Green's function $\mathcal{G}_{0,\sigma}(\omega)$ for the effective impurity in the absence of an interaction at the impurity site is given by

$$\mathcal{G}^{-1}_{0,\sigma}(\omega) = G^{\text{loc}}_\sigma(\omega)^{-1} + \Sigma_\sigma(\omega). \quad (9)$$

We can take the form of this impurity model to correspond to an Anderson model[13] in a magnetic field,

$$H_{\text{AM}} = \sum_\sigma \varepsilon_{\text{d},\sigma}d^\dagger_\sigma d_\sigma + Un_{\text{d},\uparrow}n_{\text{d},\downarrow} \quad (10)$$
$$+ \sum_{\boldsymbol{k},\sigma}(V_{\boldsymbol{k},\sigma}d^\dagger_\sigma c_{\boldsymbol{k},\sigma} + V^*_{\boldsymbol{k},\sigma}c^\dagger_{\boldsymbol{k},\sigma}d_\sigma) + \sum_{\boldsymbol{k},\sigma}\varepsilon_{\boldsymbol{k},\sigma}c^\dagger_{\boldsymbol{k},\sigma}c_{\boldsymbol{k},\sigma},$$

where $\varepsilon_{\text{d},\sigma} = \varepsilon_{\text{d}} - \sigma h$ is the energy of the localized level at an impurity site in a magnetic field $H$, $U$ the interaction at this local site, and $V_{k,\sigma}$ the hybridization matrix element to a band of conduction electrons of spin $\sigma$ with energy $\varepsilon_{\boldsymbol{k},\sigma}$. As we are focusing on an $A$ site as the impurity we take $H = H_s$.

The one-electron Green's function for the impurity site of this model is given by

$$G^{\text{imp}}_\sigma(\omega) = \frac{1}{\omega - \varepsilon_{\text{d}\sigma} - K_\sigma(\omega) - \Sigma_\sigma(\omega)}, \quad (11)$$

where

$$K_\sigma(\omega) = \sum_{\boldsymbol{k}}\frac{|V_{\boldsymbol{k},\sigma}|^2}{\omega - \varepsilon_{\boldsymbol{k},\sigma}}. \quad (12)$$

If this impurity Green's function is equated to the local lattice Green's function $G_\sigma^{\mathrm{loc}}(\omega)$, we identify $\varepsilon_{\mathrm{d}\sigma} = -\mu_\sigma$ and from equation (9), $K_\sigma(\omega)$ is given by

$$K_\sigma(\omega) = \omega + \mu_\sigma - \mathcal{G}_{0,\sigma}^{-1}(\omega). \tag{13}$$

The function $K_\sigma(\omega)$ plays the role of the effective medium and has to be calculated self-consistently.

The self-consistent calculations for $K_\sigma(\omega)$ can usually be performed iteratively. Starting from a conjectured form for $K_\sigma(\omega)$, the NRG method is used to calculate the self-energy of the effective Anderson model, from which the impurity Green's function $G_\sigma^{\mathrm{imp}}(\omega)$ in (11) and the local Green's function for the lattice $G_\sigma^{\mathrm{loc}}(\omega)$ in (8) can be deduced. If these two Green's functions do not agree, then equation (9) is used to derive a new starting value for $K_\sigma(\omega)$ and the process continued until self-consistency is achieved.

To find antiferromagnetic solutions, we calculated self-consistent solutions for a decreasing sequence of staggered magnetic fields to see if broken symmetry solutions of this type exist as the staggered field is reduced to zero. For the non-interacting density of states $\rho_0(\varepsilon)$ we take the Gaussian form $\rho_0(\varepsilon) = \mathrm{e}^{-(\varepsilon/t^*)^2}/\sqrt{\pi}t^*$, corresponding to an infinite dimensional hypercubic lattice. It is useful to define an effective bandwidth $W = 2D$ for this density of states via $D$, the point at which $\rho_0(D) = \rho_0(0)/\mathrm{e}^2$, giving $D = \sqrt{2}t^*$ corresponding to the choice in reference[14]. In all the results we present here we take the value $W = 4$. In the NRG calculations we have used the improved method[15,16] of evaluating the response functions with the complete Anders-Schiller basis[17], and also determine the self-energy from a higher order Green's function[18].

In figure 1 we show the self-consistently calculated local spectral density for the spin-up (upper panel) and spin-down electrons (lower panel) at an $A$ site with $U = 3$ and 5% hole doping (from the state at half-filling) for various values of an applied staggered field. The staggered magnetic field induces a sublattice magnetization,

$$m_A = \frac{1}{2}(n_{A,\uparrow} - n_{A,\downarrow}), \tag{14}$$

so that these spectra are quite different. For this set of parameters, this difference persists as the staggered field is reduced to zero so that we have a spontaneous sublattice magnetization corresponding to spontaneous antiferromagnetic order. For the case away from half filling, $\delta \neq 0$, we have to keep adjusting the chemical potential when iterating for a self-consistent solution. It shows a slightly oscillatory behavior when iterating for a specific filling $x$, and we follow the procedure described in reference[10]. This feature is related to the fact that instabilities to more complicated ground states for antiferromagnetic ordering than the homogeneous, commensurate one, which forms the basis for these DMFT calculation, can occur[10,19–24]. The focus of this work is, however, the analysis of generic quasiparticle properties in a doped antiferromagnetic state and we therefore consider the approach as a valid, approximate starting point
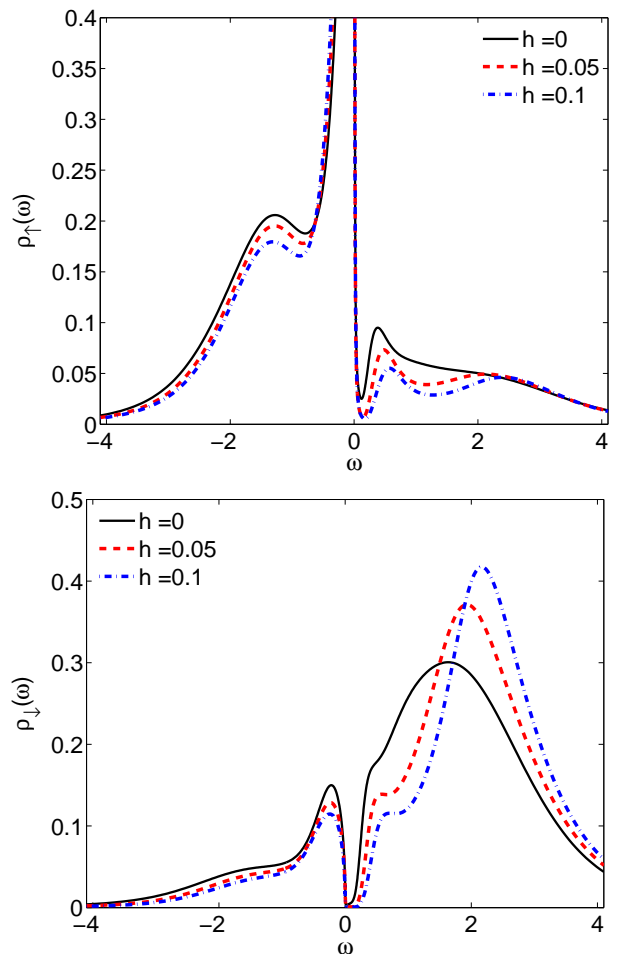


FIG. 1: (Color online) The spectral densities for the spin-up electrons (upper panel) and spin-down electrons (lower panel) at the $A$ site for various values of the applied staggered field for $U = 3$ and $x = 0.95$

for this endeavor. For a more extensive discussion of the applicability of the DMFT in this situation we refer to the earlier work[10].

From results of this type of calculation, we have built up a global antiferromagnetic/paramagnetic phase diagram as a function of the doping $\delta$ and the on-site interaction $U$. This phase diagram is shown in figure 2, where the value of the corresponding sublattice magnetization is shown in a false color plot. We have added a line separating the spontaneously ordered and paramagnetic regimes. At half filling ($\delta = 0$ axis) the spontaneous magnetization increases with $U$. This is expected to decay again for larger $U$ as the effective antiferromagnetic coupling $J$ decreases with $U$. We can see that the antiferromagnetic order from the half filled case persists when holes are added. The value of the critical doping $\delta_c$ at which the antiferromagnetism disappears depends on the on-site interaction $U$. We expect that for small $U$ the critical doping $\delta_c$ will increase with $U$ since a tendency to order only appears when an on-site interaction is present. From the mapping to the $t - J$ model we also
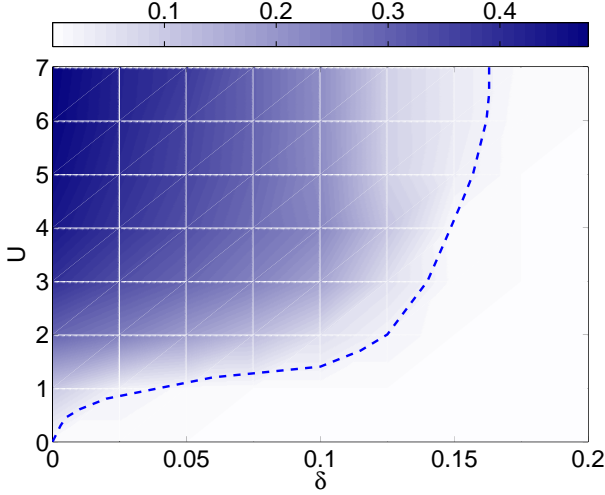
FIG. 2: (Color online) Phase diagram showing the doping and the $U$ dependence of the sublattice magnetization $m_A$ as deduced from the DMFT-NRG calculations.

expect that for large $U$ the antiferromagnetic coupling $J$ decreases and therefore the order is destroyed more easily. The values of $U$ are, however, not large enough to display this trend.

If we compare these results with the phase diagram given by Zitzler et al[10] we see that they are in very good agreement. In their case the antiferromagnetic region was mapped out to values of $U \simeq 4.5$. We have managed to extend the diagram to somewhat larger values of $U$. There is a problem of obtaining a self-consistent antiferromagnetic solution in the large $U$ regime, as the iterations tend to oscillate, as discussed by Zitzler et al.

## III. QUASIPARTICLE PARAMETERS

To examine the nature of the low energy excitations, we will assume that the self-energy $\Sigma_\sigma(\omega)$ is non-singular at $\omega = 0$ so that, at least asymptotically, it can be expanded in powers of $\omega$. This assumption is not expected to be valid close to the quantum critical point when the magnetic order sets in, but to be a reasonable assumption otherwise. We also assume that the imaginary part of the self-energy vanishes which is confirmed by the numerical results of the DMFT-NRG calculations. We will retain terms to order $\omega$ only for the moment. The higher order corrections will be considered later. We then find for $\zeta_\sigma(\omega)$,

$$\zeta_\sigma(\omega) = \omega(1 - \Sigma'_\sigma(0)) + \mu_\sigma - \Sigma_\sigma(0) \qquad (15)$$
$$= z_\sigma^{-1}(\omega + \tilde{\mu}_{0,\sigma}), \qquad (16)$$

where

$$\tilde{\mu}_{0,\sigma} = z_\sigma(\mu - \Sigma_\sigma(0)), \quad \text{and} \quad z_\sigma^{-1} = 1 - \Sigma'_\sigma(0). \quad (17)$$

The interacting Green's function (7) has poles at the roots of the quadratic equation,

$$\zeta_\sigma(\omega)\zeta_{-\sigma}(\omega) - \varepsilon_{\boldsymbol{k}}^2 = 0. \qquad (18)$$

The solutions of this equation are

$$E_{\boldsymbol{k},\pm}^0 = -\tilde{\mu} \pm \sqrt{\tilde{\varepsilon}_{\boldsymbol{k}}^2 + \Delta\tilde{\mu}^2}, \qquad (19)$$

where $\tilde{\varepsilon}_{\boldsymbol{k}} = \sqrt{z_\uparrow z_\downarrow}\varepsilon_{\boldsymbol{k}}$, $\Delta\tilde{\mu} = (\tilde{\mu}_{0,\uparrow} - \tilde{\mu}_{0,\downarrow})/2$, and $\tilde{\mu} = (\tilde{\mu}_{0,\uparrow} + \tilde{\mu}_{0,\downarrow})/2$. This has the same form as for the non-interacting system in a staggered field (5), so we can interpret these excitations as quasiparticles coupled to an effective staggered magnetic field $\tilde{h}_{\rm s} = \Delta\tilde{\mu}/g\mu_{\rm B}$, with $\tilde{\mu}$ playing the role of a quasiparticle chemical potential. This equation gives the dispersion relation for these single particle excitations, which can be regarded as constituting a renormalized band, or bands as there are two branches. The term magnetic polaron is sometimes used to describe these single particle excitations in states of magnetic order, because of the analogy with the motion of a particle in a lattice to which it is strongly coupled, where the excitation is termed a polaron.

The corresponding density of states of these free quasiparticles on the sublattice is

$$\tilde{\rho}_{0,\sigma}(\omega) = \frac{1}{\sqrt{z_\uparrow z_\downarrow}} \sqrt{\frac{\omega + \tilde{\mu} - \sigma\Delta\tilde{\mu}}{\omega + \tilde{\mu} + \sigma\Delta\tilde{\mu}}} \, \rho_0\left(\frac{\sqrt{(\omega + \tilde{\mu})^2 - \Delta\tilde{\mu}^2}}{\sqrt{z_\uparrow z_\downarrow}}\right), \qquad (20)$$

for $|\omega + \tilde{\mu}| > |\Delta\tilde{\mu}|$, and is zero otherwise. In the case of a half-filled band $\tilde{\mu} = 0$ and there is a gap at the Fermi level $\varepsilon_{\rm F} = 0$.

To determine this quasiparticle density of states in the presence of the symmetry breaking staggered magnetic field we need to calculate $z_\sigma$ and $\tilde{\mu}_{0,\sigma}$ for each spin type. Using the NRG we can do this in two ways. As the DMFT-NRG calculations give us the self-energy $\Sigma_\sigma(\omega)$ directly, we only need its value, and that of its first derivative at $\omega = 0$, to deduce both $z_\sigma$ and $\tilde{\mu}_{0,\sigma}$ using equation (17). However, because the model is solved using an effective impurity model, we can also deduce these quantities indirectly from the many-body energy levels of the impurity on approaching the low energy fixed point.[25] This second method gives us not only a check on the results of the direct method, but also allows to deduce some information about the quasiparticle interactions, as we shall show in the next section.

### A. Calculation of Renormalized Parameters

To describe how the renormalized parameters are deduced from the energy levels of the NRG calculation, we need to outline how the NRG calculations are carried out. Following the procedure introduced by Wilson[26], the conduction band is logarithmically discretized and the model then converted into the form of a one dimensional tight binding chain, coupled via an effective hybridization $V_\sigma$ to the impurity at one end. In this representation $K_\sigma(\omega) = |V_\sigma|^2 g_{0,\sigma}^{(N)}(\omega)$, where $g_{0,\sigma}^{(N)}(\omega)$ is the one-electron Green's function for the first site of the isolated conduction electron chain of length $N$. The impurity Green's function for this discretized model then

takes the form,

$$G_\sigma^{\text{imp}}(\omega) = \frac{1}{\omega - \varepsilon_{\text{d}\sigma} - |V_\sigma|^2 g_{0,\sigma}^{(N)}(\omega) - \Sigma_\sigma(\omega)}. \quad (21)$$

We can find the quasiparticle excitations of this model by expanding the self-energy $\Sigma_\sigma(\omega)$ in the denominator of this equation to first order in $\omega$, and write the result in the form,

$$G_\sigma^{\text{imp}}(\omega) = \frac{z_\sigma}{\omega - \tilde{\varepsilon}_{\text{d}\sigma} - |\tilde{V}_\sigma|^2 g_{0,\sigma}^{(N)}(\omega) + \mathcal{O}(\omega^2)}, \quad (22)$$

where

$$\tilde{\varepsilon}_{\text{d}\sigma} = z_\sigma[\varepsilon_{\text{d}\sigma} + \Sigma_\sigma(0)], \quad |\tilde{V}_\sigma|^2 = z_\sigma|V_\sigma|^2. \quad (23)$$

We can then define a free quasiparticle propagator, $\tilde{G}_{0,\sigma}(\omega)$, viz

$$\tilde{G}_{0,\sigma}^{\text{imp}}(\omega) = \frac{1}{\omega - \tilde{\varepsilon}_{\text{d}\sigma} - |\tilde{V}_\sigma|^2 g_{0,\sigma}^{(N)}(\omega)}, \quad (24)$$

and interpret $z_\sigma$ as the quasiparticle weight.

In the NRG calculation the many-body excitations are calculated iteratively, starting at the impurity site, and increasing the chain length $N$ by one site with each iteration. When the matrices become too large to handle, only the lowest 500-1500 states are kept at each iteration. The many-body energy levels for the $N$th iteration and the set of quantum numbers $M$, $E_M(N)$, depend on the chain length $N$ and the discretization parameter $\Lambda > 1$. When $N$ becomes large these energy levels go to zero as $\Lambda^{-N/2}$. We now conjecture that the lowest single particle $E_p^\sigma(N)$ and single hole excitations $E_h^\sigma(N)$ determined from the NRG many-body excitations correspond to quasiparticle excitations. If this is the case then they should correspond to the poles of the quasiparticle Green's function given in equation (24), with values of $\tilde{V}_\sigma$ and $\tilde{\varepsilon}_{\text{d}\sigma}$, which are independent of $N$ as $N \to \infty$. We can test this hypothesis by substituting the values, $\omega = E_p^\sigma(N)$ and $\omega = E_h^\sigma(N)$, into the equation,

$$\omega - \tilde{\varepsilon}_{\text{d}\sigma} - |\tilde{V}_\sigma|^2 g_{0,\sigma}^{(N)}(\omega) = 0, \quad (25)$$

and deduce values of $\tilde{V}_\sigma$ and $\tilde{\varepsilon}_{\text{d}\sigma}$, which will in general depend upon $N$. From these we can deduce $z_\sigma = |\tilde{V}_\sigma/V_\sigma|^2$ and $\tilde{\mu}_{0,\sigma} = -\tilde{\varepsilon}_{\text{d}\sigma}$, which will also depend upon $N$, but if the lowest single particle excitations of the system do correspond to free quasiparticles, the values of $z_\sigma$ and $\tilde{\mu}_{0,\sigma}$ will become independent of $N$ for large $N$. It should be noted that we need both the particle and hole excitations for each spin to determine the four renormalized parameters. The parameters corresponding to spin up involve the particle excitations with spin up and the hole excitations with spin down.

That parameters can be found, which are independent of $N$ for large $N$, can be seen in figure 3, where we take the results of a $K_\sigma(\omega)$ and $\mu_\sigma$ from the antiferromagnetic
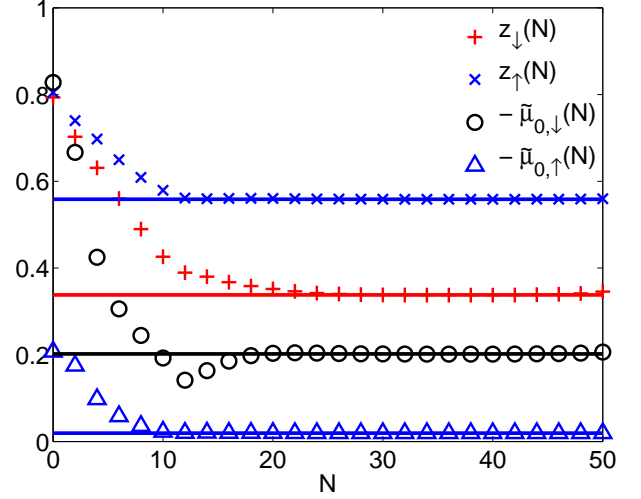


FIG. 3: (Color online) The $N$-dependence of the renormalized parameters $z_\sigma$ and $\tilde{\mu}_{0,\sigma}$ for $U = 3$ and $x = 0.9$

self-consistent solution for the Hubbard model with $U = 3$ and 10% doping, using a value for the discretization parameter $\Lambda = 1.8$.

It can be seen that after about 25 iterations all the values deduced for $z_\sigma$ and $\tilde{\mu}_{0,\sigma}$ become independent of $N$. In the next section, where we compare these results with the corresponding values deduced directly from the self-energy, we get further confirmation that the values deduced really do describe the quasiparticle excitations of the lattice model.

When two or more quasiparticles are excited from the interacting ground state, there will be an interaction between them. For the Anderson impurity model this interaction will be local and can be expressed as $\tilde{U}$, a renormalized value of the original interaction of the 'bare' particles. The value of $\tilde{U}$ can be deduced by looking at lowest lying two-particle excitations derived from NRG calculation. These could either be two-particle excitations, $E_{pp}^{\uparrow,\downarrow}(N)$, two-hole excitations, $E_{hh}^{\downarrow,\uparrow}(N)$ or a particle-hole excitation $E_{ph}^{\uparrow,\uparrow}(N)$. By looking at the difference between a two-particle excitation and two single particle excitations, $E_{pp}^{\uparrow,\downarrow}(N) - E_p^\uparrow(N) - E_p^\downarrow(N)$, as a function of $N$ we can deduce an effective interaction $\tilde{U}_{pp}^{\uparrow,\downarrow}(N)$ between these two quasiparticles, as has been described fully earlier for the standard Anderson model.[25] In a similar way we can deduce an effective interaction between two holes, $\tilde{U}_{hh}^{\downarrow,\uparrow}(N)$, or a particle and hole, $-\tilde{U}_{ph}^{\uparrow,\uparrow}(N)$. To be able to define a single quasiparticle interaction $\tilde{U}$, not only must $\tilde{U}_{pp}^{\uparrow,\downarrow}(N)$, $\tilde{U}_{hh}^{\downarrow,\uparrow}(N)$ and $\tilde{U}_{ph}^{\uparrow,\uparrow}(N)$, give values which are independent of $N$ for large $N$, $\tilde{U}_{pp}^{\uparrow,\downarrow}$, $\tilde{U}_{hh}^{\downarrow,\uparrow}$ and $\tilde{U}_{ph}^{\uparrow,\uparrow}$, these values must be equal so $\tilde{U}_{pp}^{\uparrow,\downarrow} = \tilde{U}_{hh}^{\downarrow,\uparrow} = \tilde{U}_{ph}^{\uparrow,\uparrow} = \tilde{U}$. In figure 4 we give the values of $\tilde{U}_{pp}^{\uparrow,\downarrow}(N)$, $\tilde{U}_{hh}^{\downarrow,\uparrow}(N)$ and $\tilde{U}_{ph}^{\uparrow,\uparrow}(N)$ as deduced from DMFT-NRG calculation for the Hubbard model in an antiferromagnetic state with $U = 6$, 10% doping and $\Lambda = 1.8$. It can be seen that the three sets of results settle down to common value $\tilde{U}$.
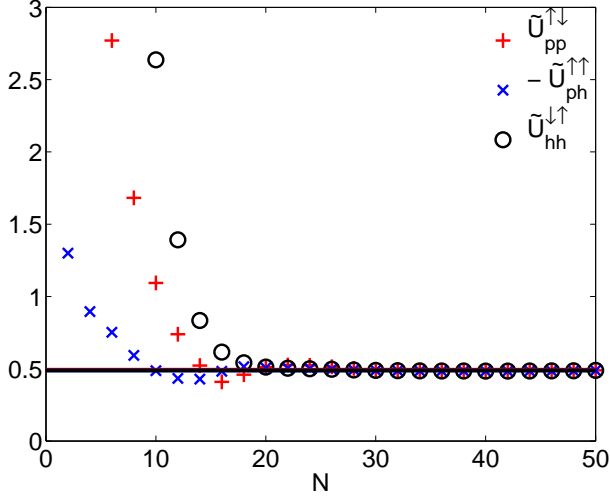
FIG. 4: (Color online) The $N$-dependence of the renormalized particle-particle, particle-hole and hole-hole interactions for $U = 6$ and $x = 0.9$, showing that they converge to a unique value $\tilde{U}$.

We can go further and identify $\tilde{U}$ with the local quasiparticle 4-vertex interaction for the effective impurity model,

$$\tilde{U} = z_\uparrow z_\downarrow \Gamma_{\uparrow,\downarrow,\downarrow,\uparrow}(0,0,0,0), \qquad (26)$$

where $\Gamma_{\uparrow,\downarrow,\downarrow,\uparrow}(\omega_1, \omega_2, \omega_3, \omega_4)$ is the total 4-vertex at the impurity site, which is equal to the same quantity for a site in the lattice model. With this interpretation it is possible to identify these parameters with those used in a renormalized perturbation expansion. The parameters, $V$, $\varepsilon_{d,\sigma}$ and $U$, together with $g_{0,\sigma}^N(\omega)$, specify the effective impurity model. The renormalized parameters, $\tilde{V}$, $\tilde{\varepsilon}_{d,\sigma}$ and $\tilde{U}$, together with $g_{0,\sigma}^N(\omega)$, can be used as an alternative way of specifying this model. The renormalized perturbation theory (RPT) is set up by expanding the self-energy to order $\omega$, as earlier, but retaining all the higher order correction terms in a remainder term,

$$\Sigma_\sigma(\omega) = \Sigma_\sigma(0) + \omega \Sigma_\sigma'(0) + \Sigma_\sigma^{\text{rem}}(\omega), \qquad (27)$$

where $\Sigma_\sigma^{\text{rem}}(\omega)$ is the remainder term. On substituting this into the equation for the impurity Green's function in equation (11), we can deduce a general expression for the quasiparticle Green's function in the form,

$$\tilde{G}_\sigma^{\text{imp}}(\omega) = \frac{1}{\omega - \tilde{\varepsilon}_{d\sigma} - \tilde{K}_\sigma(\omega) - \tilde{\Sigma}_\sigma(\omega)}, \qquad (28)$$

where $\tilde{K}_\sigma(\omega) = z_\sigma K_\sigma(\omega)$ and $\tilde{\Sigma}_\sigma(\omega) = z_\sigma \Sigma_\sigma^{\text{rem}}(\omega)$ plays the role of a renormalized self-energy. A diagrammatic perturbation theory can then be carried out for $\tilde{\Sigma}_\sigma(\omega)$ in terms of the free quasiparticle propagators, with additional diagrams arising from counter terms, which are required to prevent over-counting (renormalization conditions).[9,27,28] This form of perturbation theory is valid for all energy scales but is particularly effective for

calculating the low energy terms arising from the quasiparticle interactions. For the symmetric Anderson impurity model it has been shown that this perturbation theory taken to second order in $\tilde{U}$, gives the exact spin and charge susceptibilities at $T = 0$, and the exact $T^2$ contribution to the conductivity.[9]

Because, within DMFT, the self-energy for the lattice is the same as that for the effective impurity, we can equally well use the effective impurity model to calculate it. This means that we can use the renormalized perturbation theory for the effective impurity model to estimate the correction terms to the free quasiparticle picture arising from the quasiparticle interactions.

## B. Quasiparticle weight

We now consider the values of the quasiparticle weight factor $z_\sigma$, commonly known also as the wavefunction renormalization factor. This is an important factor in determining the parameters needed to describe the low energy behavior of the system. When there is no $\boldsymbol{k}$-dependence of the self-energy, as is the case for infinite dimensional models and DMFT, the effective mass of the quasiparticles in the paramagnetic state is proportional to $1/z_\sigma$. We show later that in the antiferromagnetic state $1/\sqrt{z_\uparrow z_\downarrow}$ plays the corresponding role. We have determined this quantity from the NRG results by the two methods described and give the values of $z_\sigma$ deduced for both spin types as a function of doping in figure 5. The results are for the case $U = 3$, where there is antiferromagnetic order and the external staggered field has been set to zero.
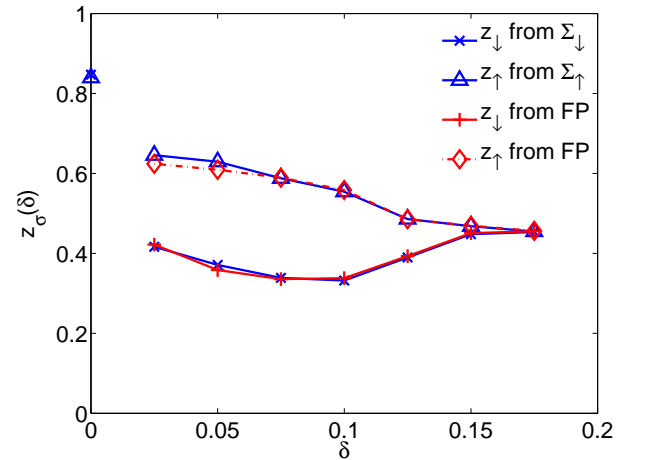


FIG. 5: (Color online) The quasiparticle weight $z_\sigma$ as deduced directly from the self-energy and also from the impurity fixed point (FP) for $U = 3$ and various dopings.

It can be seen that there is a reasonable agreement between the values obtained by the two different methods of calculation. For the half filled case $\delta = 0$, the system has a gap and there is no unique value for the Fermi

energy. We have in this case taken values $z_\sigma$ only from the derivative of the self-energy at $\omega = 0$. Here due to particle-hole symmetry $z_\uparrow = z_\downarrow$, and the value at his point 0.85 indicates a very modest degree of renormalization. For comparison we note that in the paramagnetic phase, if we do not allow for antiferromagnetic order, we have the smaller value $z_\sigma \simeq 0.47$. The antiferromagnetic order seems to have the tendency to decrease renormalization effects at half filling. When the system is doped but still ordered, however, $z_\uparrow \neq z_\downarrow$, and the renormalization effects are much stronger especially for the minority (down) spin particles on the sublattice. This is similar to the results we found for a doped Hubbard model in a paramagnetic state in the presence of a strong uniform magnetic field[8]. For certain range of dopings the values of $z_\uparrow$ and $z_\downarrow$ do not vary much. The tendency is that $z_\downarrow$ first decreases and later increases, whereas $z_\uparrow$ decreases over the whole range until both of them merge at the doping point where the antiferromagnetic order disappears. In the ordered phase the term $\sqrt{z_\uparrow z_\downarrow}$ does not change much when the doping is increased. This is in contrast to the paramagnetic phase where the corresponding values $z_\sigma$ increases with the doping.

The results for the corresponding case with $U = 6$, a value which is larger than the bandwidth, are shown in figure 6.
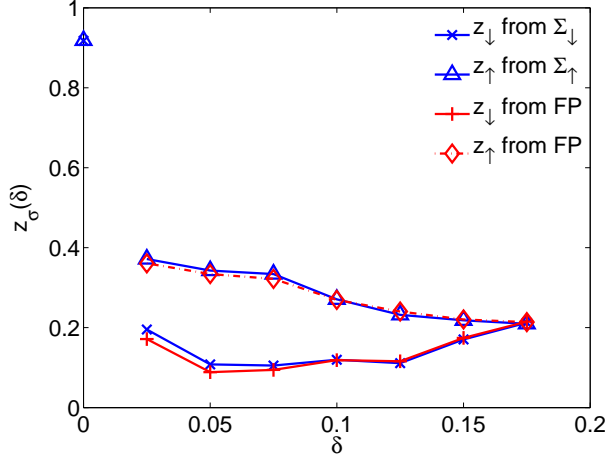


FIG. 6: (Color online) The quasiparticle weight $z_\sigma$ as deduced directly from the self-energy and from the impurity fixed point (FP) for $U = 6$ and various dopings.

On the whole the behavior is quite similar to that for the case $U = 3$, only that the renormalization effects are more pronounced. For half filling this is in strong contrast with the non-ordered paramagnetic state which would be a Mott insulator for $U = 6$ with $z_\sigma = 0$. Away from half filling, for a range of dopings the quasiparticle weights do not change much and have the same tendency as described above. If we compare again to the paramagnetic phase, for instance, for 5% doping we have $z_\sigma \simeq 0.097$, whereas in the antiferromagnetic phase $\sqrt{z_\uparrow z_\downarrow} \simeq 0.196$ signaling a smaller effective mass there. This is discussed in more detail later.

## C. Renormalized chemical potential

In figure 7 we give the results for the renormalized chemical potential, $\tilde{\mu}_{0,\sigma}$ [defined in equation (17) and (23)], for the two spin types in the spontaneously ordered antiferromagnetic states for $U = 3$ and $U = 6$ for a range of dopings.
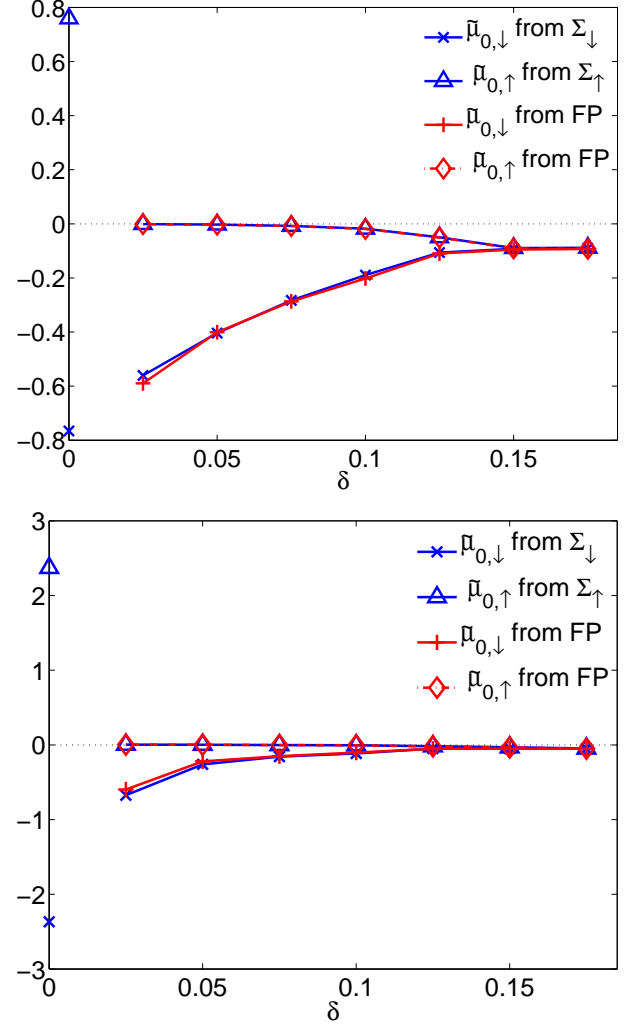


FIG. 7: (Color online) The renormalized chemical potential $\tilde{\mu}_{0,\sigma}$ as deduced directly from the self-energy and from the impurity fixed point (FP) for various dopings for $U = 3$ (upper panel) and $U = 6$ (lower panel).

The values calculated by the two different methods can be seen to be in good agreement here, as well. We have added the values for the half filled case. These were calculated from the self-energy in the gap at $\omega = 0$. The general behavior of the values for $\tilde{\mu}_{0,\sigma}$ for the case with $U = 6$ is very similar to the case with smaller $U$, with again good agreement between the two sets determined by the different methods.

The renormalized chemical potential $\tilde{\mu}_{0,\sigma}$ is an important parameter in specifying the form of the sublattice quasiparticle spectral density $\tilde{\rho}_\sigma^0(\omega)$. From equation (20)

it can be seen that, as $\omega \rightarrow -\tilde{\mu}_{0,\sigma}$, $\tilde{\rho}_{0,\sigma}(\omega)$ behaves asymptotically as

$$\tilde{\rho}_{0,\sigma}(\omega) \sim \frac{1}{\sqrt{\omega + \tilde{\mu}_{0,\sigma}}}, \qquad (29)$$

so the quasiparticle density of states has a square root singularity at $\omega = -\tilde{\mu}_{0,\sigma}$. On the other hand, however, as $\omega \rightarrow -\tilde{\mu}_{0,-\sigma}$, $\tilde{\rho}_{0,\sigma}(\omega)$ behaves as

$$\tilde{\rho}_{0,\sigma}(\omega) \sim \sqrt{\omega + \tilde{\mu}_{0,-\sigma}}, \qquad (30)$$

so the quasiparticle density of states goes to zero at $\omega = -\tilde{\mu}_{0,-\sigma}$. Between the two points, $\omega = -\tilde{\mu}_{0,\sigma}$ and $\omega = -\tilde{\mu}_{0,-\sigma}$, the quasiparticle density of states has a gap $2\Delta\tilde{\mu}$. As can be seen in figure 7 this free quasiparticle gap decreases with the doping and closes in the param-agnetic state. If we take into account the values at half filling we see a strong reduction of $2\Delta\tilde{\mu}$, when doping the system. We also see that $\tilde{\mu}_{0,\uparrow}$ drops to small negative values for finite hole doping, which corresponds to the fact that the Fermi level then lies within the lower band. These features will be seen clearly in the figures presented in the next section, where we compare the quasiparticle densities of states with the full local spectral densities calculated from the DMFT-NRG.

### D.   The quasiparticle interaction

The quasiparticles can be further characterized by an effective interaction $\tilde{U}$ as described before. In figure 8 we plot the doping dependence of the renormalized interaction over a range of dopings and $U = 3$ and $U = 6$.
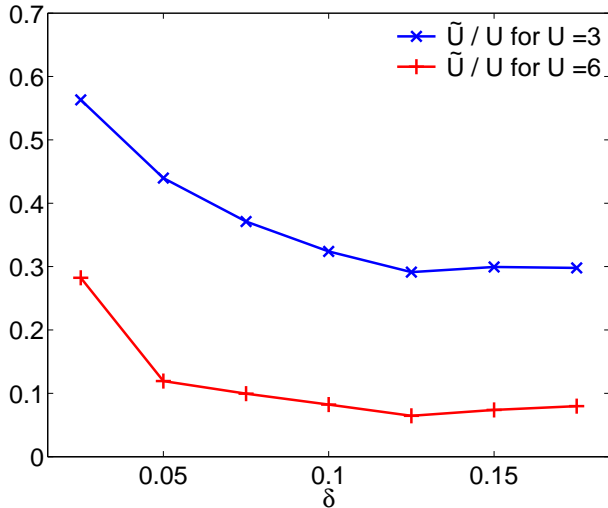


FIG. 8: (Color online) The renormalised quasiparticle interaction $\tilde{U}/U$ as deduced from the impurity fixed point for various dopings and $U = 3, 6$.

We can see that in both cases the values decrease with increasing doping. Hence, the effective quasiparticle interaction is stronger for a smaller hole density. For a certain range of dopings $\tilde{U}$ does, however, not vary much.

We can also see that the the ratio $\tilde{U}/U$ for the effective interaction assume smaller values the larger the bare $U$ becomes. Also the absolute value of $\tilde{U}$, i.e. without the scaling with $U$ as in figure 8, is smaller for larger bare $U$ for the full range of dopings. This effect of smaller quasiparticle interactions for the stronger coupling case can be seen as sharper quasiparticle peaks for larger $U$ as will be discussed in the next section.

## IV.   SPECTRA AND QUASIPARTICLE BANDS

### A.   Local Spectra

In this section we examine how well the sublattice quasiparticle density of states $\tilde{\rho}_{0,\sigma}(\omega)$, evaluated from equation (20) with the renormalised parameters, de-scribes the low energy features seen in the local spectral density $\rho_\sigma(\omega)$ calculated from the DMFT-NRG. At half filling there is a gap at the Fermi level, so there are no single particle excitations in the immediate neighbour-hood of the Fermi level, and this is not a very interesting case to consider. We look in detail at the case of 10% doping where the Fermi level lies at the top of the lower band, and consider the two cases $U = 3$ and $U = 6$. In the upper panel of figure 9 we compare the spectral density $\rho_\uparrow(\omega)$ with the corresponding quantity $z_\uparrow\tilde{\rho}_{0,\uparrow}(\omega)$, from the quasiparticle density of states.

We see that the behavior near the Fermi level ($\omega = 0$), and the singular feature seen in the lower branch of $\rho_\uparrow(\omega)$, are well reproduced by the quasiparticle density of states. Above the Fermi level there is a peak in the quasiparti-cle density of states similar to that in the full spectrum but somewhat more pronounced. Above the Fermi level and below the upper peak there is a pseudo-gap region. In the free quasiparticle spectrum it is a definite gap. In the spectrum calculated from the direct NRG evalua-tion it appears as a pseudo-gap, with rather small spec-tral weight just above the Fermi level. From the direct DMFT-NRG calculations, due to the broadening features introduced to obtain a continuous spectrum, it is not al-ways possible to say definitively whether there is a true gap above the Fermi level or not. To resolve this question we can appeal to the renormalised perturbation theory to look at the corrections to the quasiparticle density of states arising from the quasiparticle interactions. A cal-culation of the imaginary part of the renormalised self-energy $\tilde{\Sigma}_\sigma(\omega)$ to order $\tilde{U}^2$ should be sufficient to settle this issue. The imaginary part of the second order dia-gram for the renormalised self-energy in the limit $T \rightarrow 0$ for $\omega > 0$ is given by

$$\mathrm{Im}\tilde{\Sigma}_\sigma^{(2)}(\omega) = \pi\tilde{U}^2 \int_0^\omega d\varepsilon_1 \int_0^{-\omega} d\varepsilon_2 \, \tilde{\rho}_{0,\sigma}(\varepsilon_1)\tilde{\rho}_{0,-\sigma}(\omega - \varepsilon_1 + \varepsilon_2)$$
$$\times \, \tilde{\rho}_{0,-\sigma}(\varepsilon_2)\theta(\omega - \varepsilon_1 + \varepsilon_2), \qquad (31)$$

where $\tilde{\rho}_{0,\sigma}(\varepsilon)$ is the free quasiparticle density of states.
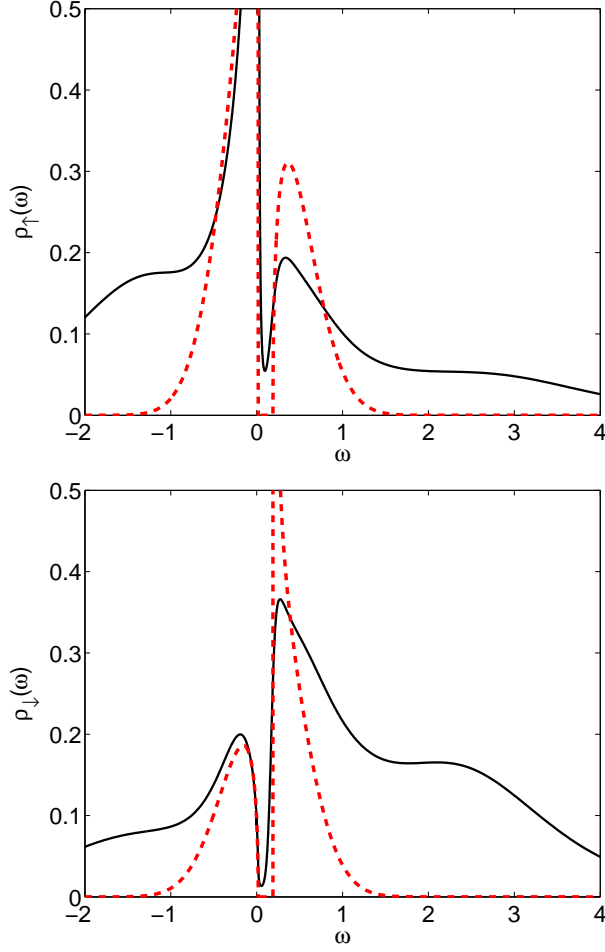
FIG. 9: (Color online) The free quasiparticle spectrum (dashed line) in comparison with DMFT-NRG spectrum for $x = 0.9$ and $U = 3$ for the spin-up electrons (majority, upper panel) and spin-down electrons (minority, lower panel).

The integration area is a triangle in the $(\varepsilon_1, \varepsilon_2)$-plane as shown in figure 10.

To analyze the behavior of $\mathrm{Im}\tilde{\Sigma}_\sigma^{(2)}(\omega)$ in the regime $|\tilde{\mu}_{0,\uparrow}| < \omega < |\tilde{\mu}_{0,\downarrow}|$ we have to study where the integrand is non-zero taking into account that $\tilde{\rho}_{0,\sigma}(\varepsilon) = 0$ for $|\tilde{\mu}_{0,\uparrow}| < \varepsilon < |\tilde{\mu}_{0,\downarrow}|$. The only non-zero contribution comes from the small shaded region in figure 10, which leads to the estimate,

$$\mathrm{Im}\tilde{\Sigma}_\sigma^{(2)}(\omega) \simeq \pi \tilde{U}^2 \tilde{\rho}_{0,\sigma}(0) \tilde{\rho}_{0,-\sigma}(-\omega) \tilde{\rho}_{0,-\sigma}(0) \tilde{\mu}_{0,\uparrow}^2. \quad (32)$$

When $\tilde{\mu}_{0,\uparrow}$ is small, which occurs when the lower edge of the gap in the quasiparticle density of states is very near the Fermi level, this contribution to the imaginary part of the renormalized self-energy will be finite but small. It decreases with $\omega$ due the behavior of $\tilde{\rho}_{0,-\sigma}(-\omega)$. Based on this argument we conclude that there is a small, but finite imaginary part of the self-energy in the free quasiparticle gap $2\Delta\tilde{\mu}$, when it lies above the Fermi level, giving rise to a finite spectral weight there. However, this spectral weight is very small close to the lower edge of
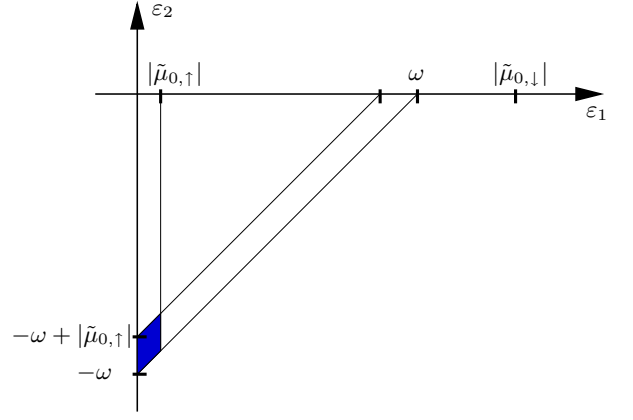


FIG. 10: (Color online) Integration region in the $(\varepsilon_1, \varepsilon_2)$-plane for the imaginary part of the self-energy. The original triangle region $(0, \omega, -\omega)$ for integration in equation (31) is reduced in the gap region $|\tilde{\mu}_{0,\uparrow}| < \omega < |\tilde{\mu}_{0,\downarrow}|$ to the small shaded region shown in the figure.

the free quasiparticle density of states, when this edge lies only just above the Fermi level.

In the lower panel of figure 9 we compare the $\rho_\downarrow(\omega)$ with $z_\downarrow \tilde{\rho}_{0,\downarrow}(\omega)$. We see that in this case also the quasiparticle density of states reproduces well the spectrum in the region of the Fermi level and the peak structure in the lower band, which is non-singular in this case. The position of the peak above the Fermi level is also well reproduced, but the peak in the free quasiparticle density of states is singular, whereas that in the DMFT-NRG results is not. We would expect to lose this singularity in the free quasiparticle density of states once the quasiparticle scattering is taken into account and the renormalized self-energy is included. It is possible also that the peak above the Fermi level in the DMFT-NRG spectrum should be sharper, as there is some tendency for the broadening introduced in this approach to flatten peaked features in regions away from the Fermi level. The spectral weight in the pseudo-gap is even smaller than in the case for the spin-up electrons, particularly in the region of the gap that lies closest to the Fermi level. This is qualitatively in line with the conclusions based on the renormalized perturbation theory estimate of the effects of the quasiparticle scattering.

We see very similar features in the spectra for the case $U = 6$ and also 10% doping shown in figure 11.

Here, the peaks near the Fermi level are a bit sharper. The observations made on the comparison of the quasiparticle and DMFT-NRG spectra apply equally well to this case. In addition to the low energy charge peaks corresponding to the Hubbard bands. The lower one can be identified in the full spectra, whereas the upper Hubbard peak is not seen on the energy scale shown. The quasiparticle density of states, of course does not contain information about these features at higher energy.
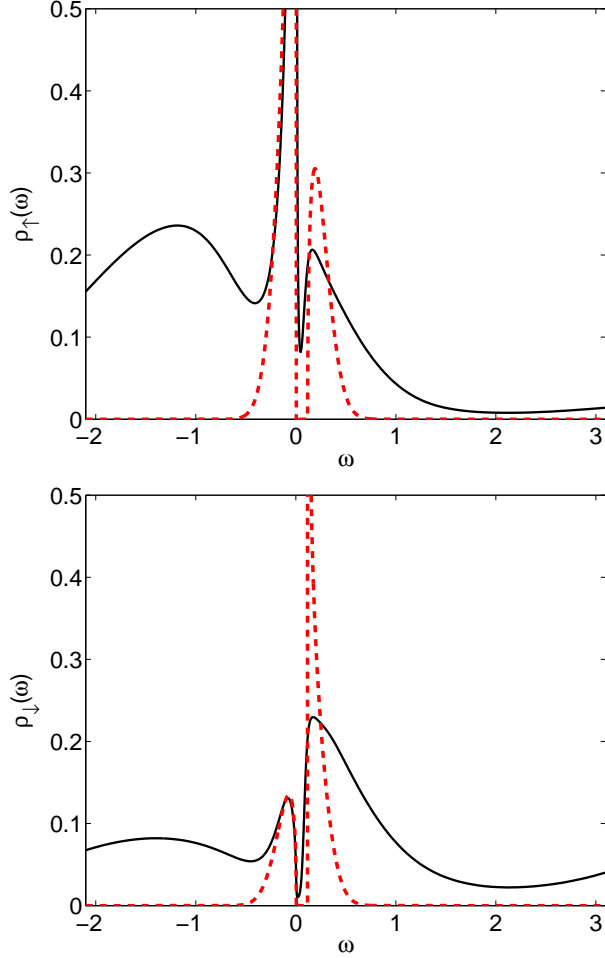
FIG. 11: (Color online) The free quasiparticle spectrum (dashed line) in comparison with DMFT-NRG spectrum for $x = 0.9$ and $U = 6$ for the spin-up electrons (upper panel) and spin-down electrons (lower panel).

## B. $k$-resolved Spectra

We can learn more about the low energy single particle excitations by looking at the spectral density of the Green's function $\underline{G}_{\boldsymbol{k},\sigma}(\omega)$ in equation (7) for a given wave-vector $\boldsymbol{k}$. With the self-energies $\Sigma_\sigma(\omega)$ calculated within the DMFT-NRG approach all elements of this matrix can be evaluated. The local spectra and self-energies are spin-dependent in the doped broken symmetry state, however, the free quasiparticle bands $E^0_{\boldsymbol{k},\pm}$ [equation (19)] do not depend on the spin. Here, we focus on the diagonal part of $\underline{G}_{\boldsymbol{k},\sigma}(\omega)$ corresponding to the $A$ sublattice,

$$G_{\boldsymbol{k},\sigma}(\omega) = \frac{\zeta_{-\sigma}(\omega)}{\zeta_\sigma(\omega)\zeta_{-\sigma}(\omega) - \varepsilon_k^2}. \qquad (33)$$

The weights of the quasiparticle excitations in this case depend on the spin corresponding to the sublattice properties. We note that one can also analyze the quasiparticle bands differently, for instance, from the $\boldsymbol{k}$-resolved

spectra and the diagonal form of $\underline{G}_{\boldsymbol{k},\sigma}(\omega)$. The form of the quasiparticle bands remains unchanged then, but the weights differ and do not depend on the spin $\sigma$ in that case.

We first of all look at the Fermi surface which is the locus of the $\boldsymbol{k}$-points at the Fermi level ($\omega = 0$) where the Green's function has poles. The conduction electron energy $\varepsilon_{\boldsymbol{k}_{\mathrm{F}}}$ at these point is given by

$$\varepsilon^2_{\boldsymbol{k}_{\mathrm{F}}} = (\mu_\uparrow - \Sigma_\uparrow(0))(\mu_\downarrow - \Sigma_\downarrow(0)). \qquad (34)$$

By Luttinger's theorem, the volume of the Fermi surface for the interacting system must equal that for the non-interacting system with the same density. As the self-energy depends only on $\omega$, the two Fermi surfaces must also have the same shape, and therefore must be identical. The Fermi surface of the non-interacting system is given by $\varepsilon_{\boldsymbol{k}_{\mathrm{F}}} = \mu_0$, where $\mu_0$ is the chemical potential of the non-interacting system in the absence of any applied field for the given density. For this to be identical with that given in equation (34),

$$(\mu_\uparrow - \Sigma_\uparrow(0))(\mu_\downarrow - \Sigma_\downarrow(0)) = \mu_0^2. \qquad (35)$$

We can check that this relation indeed holds from our results for $\Sigma_\sigma(\omega)$ and $\mu_\sigma$, independent of the value of $U$, or in the case of an applied staggered field, independent of the field value. This relation implies that the total number of electrons per site $n$ can be calculated from an integral over the non-interacting density of states,

$$n = 2 \int_{-\infty}^{\mu_0} \rho_0(\omega)d\omega, \qquad (36)$$

where in the hole doped case $\mu_0 = -\sqrt{\bar{\mu}_\uparrow \bar{\mu}_\downarrow}$ and $\bar{\mu}_\sigma = \mu_\sigma - \Sigma_\sigma(0)$).

To relate this result to the quasiparticle picture, we expand the self-energy in equation (33) to first order in $\omega$, but retain the remainder term, $\Sigma^R_\sigma(\omega)$ as in equation (27). The Green's function can be rewritten in the form,

$$\tilde{G}_{\boldsymbol{k},\sigma}(\omega) = \frac{\tilde{\zeta}_{-\sigma}(\omega)}{\tilde{\zeta}_\sigma(\omega)\tilde{\zeta}_{-\sigma}(\omega) - \tilde{\varepsilon}_{\boldsymbol{k}}^2}, \qquad (37)$$

where $\tilde{\zeta}_\sigma(\omega) = \omega + \tilde{\mu}_{0,\sigma} - \tilde{\Sigma}_\sigma(\omega)$. We define a quasiparticle Green's function $\tilde{G}_{\boldsymbol{k},\sigma}(\omega)$ via $z_\sigma \tilde{G}_{\boldsymbol{k},\sigma}(\omega) = G_{\boldsymbol{k},\sigma}(\omega)$. The renormalised self-energy vanishes, $\tilde{\Sigma}_\sigma(\omega) = 0$, for the free quasiparticle Green's function $\tilde{G}^{(0)}_{\boldsymbol{k},\sigma}(\omega)$, which can be separated into two independent branches of free quasiparticles,

$$\tilde{G}^{(0)}_{\boldsymbol{k},\sigma}(\omega) = \frac{u^\sigma_+(\varepsilon_{\boldsymbol{k}})}{\omega - E^0_{\boldsymbol{k},+}} + \frac{u^\sigma_-(\varepsilon_{\boldsymbol{k}})}{\omega - E^0_{\boldsymbol{k},-}}, \qquad (38)$$

where $E^0_{\boldsymbol{k},\pm}$ was defined in equation (19) and the weights are given by

$$u^\sigma_\pm(\varepsilon_{\boldsymbol{k}}) = \frac{1}{2}\left(1 \mp \sigma \frac{\Delta\tilde{\mu}}{\sqrt{\Delta\tilde{\mu}^2 + \tilde{\varepsilon}_{\boldsymbol{k}}^2}}\right). \qquad (39)$$

This is similar in form to mean field theory, which would correspond to putting $z_\sigma = 1$, and $\Delta\tilde\mu = Um_{\mathrm{mf}}$, where $m_{\mathrm{mf}}$ is the mean field sublattice magnetisation.

The spectral density $\tilde\rho_{\boldsymbol{k}}^{(0)}(\omega)$ for this free quasiparticle Green's function is a set of delta-functions,

$$\tilde\rho_{\boldsymbol{k},\sigma}^{(0)}(\omega) = u_+^\sigma(\varepsilon_{\boldsymbol{k}})\delta(\omega-E_{\boldsymbol{k},+}^0)+u_-^\sigma(\varepsilon_{\boldsymbol{k}})\delta(\omega-E_{\boldsymbol{k},-}^0). \quad (40)$$

On the Fermi surface $E_{\boldsymbol{k},-}^0 = 0$, which is consistent with the result for the Fermi surface given in equation (34). Summing over $\boldsymbol{k}$ gives the local quasiparticle density of states in equation (20). We define the quasiparticle number $\tilde n$ as the integral of the sum of the spin up and spin down quasiparticle density of states up to the Fermi level,

$$\tilde n = \frac{2}{\sqrt{z_\uparrow z_\downarrow}}\int\limits_{-\infty}^{0}\frac{d\omega(\omega+\tilde\mu)}{\sqrt{(\omega+\tilde\mu)^2-\Delta\tilde\mu^2}}\rho_0\left(\frac{\sqrt{(\omega+\tilde\mu)^2-\Delta\tilde\mu^2}}{\sqrt{z_\uparrow z_\downarrow}}\right).$$
$$(41)$$

If we change the variable of integration to $\omega'$, where $\omega'\sqrt{z_\uparrow z_\downarrow} = \sqrt{(\omega+\tilde\mu)^2-\Delta\tilde\mu^2}$, the integration can be shown to be identical with that in equation (36), using the fact that $\mu_0 = -\sqrt{\bar\mu_\uparrow\bar\mu_\downarrow}$. We then have an alternative statement of Luttinger's theorem in the form $\tilde n = n$. This can also be found by summing both spin components in (40), integrating over $\omega$ and then converting the $\boldsymbol{k}$-summation to an integral over the free electron density of states $\rho_0(\omega)$. We can check in our numerical results that the relation in this form holds. The occupation number $n$ can be calculated both from a direct evaluation of the number operator in the ground state, and also by integrating the sum of the spectral densities $\rho_\sigma(\omega)$ of the full local Green's function to the Fermi level. The value of $\tilde n$ is similarly determined from the integral over the total quasiparticle density of states, $\tilde\rho_\sigma(\omega)$. All three results were found to be in good agreement, to within one or two percent deviation at the most.

In order to understand better the properties of the quasiparticle bands, we now compare the quasiparticle spectrum with $\boldsymbol{k}$-resolved spectral density $\rho_{\boldsymbol{k},\sigma}(\omega)$ derived from the DMFT-NRG results.

In figure 12 we make a comparison for the case of 12.5% doping with $U = 3$ for the Green's function $G_{\boldsymbol{k},\sigma}(\omega)$ given in equation (33), $\rho_{\boldsymbol{k},\sigma}(\omega) = -\mathrm{Im}G_{\boldsymbol{k},\sigma}(\omega^+)/\pi$, where $\omega^+ = \omega + i\eta$, with $\eta \to 0$, with that derived for the free quasiparticles, $z_\sigma\tilde\rho_{\boldsymbol{k},\sigma}^{(0)}(\omega)$ from equation (40). The delta-functions of the free quasiparticle results are indicated by arrows with the height of the arrow indicating the value of the corresponding spectral weight. The plots as a function of $\omega$ are shown for a sequence values of $\varepsilon_{\boldsymbol{k}}$ and, where the peaks in $\rho_{\boldsymbol{k},\sigma}(\omega)$ get very narrow and high in the vicinity of the Fermi level, they have been truncated. It can be seen that the free quasiparticle results give a reasonable picture of the form of $\rho_{\boldsymbol{k},\sigma}(\omega)$, particularly in the immediate region of the Fermi level. There is considerable variation along the curves in the way the overall spectral weight is distributed between the excitations below and above the pseudo-gap as a function of
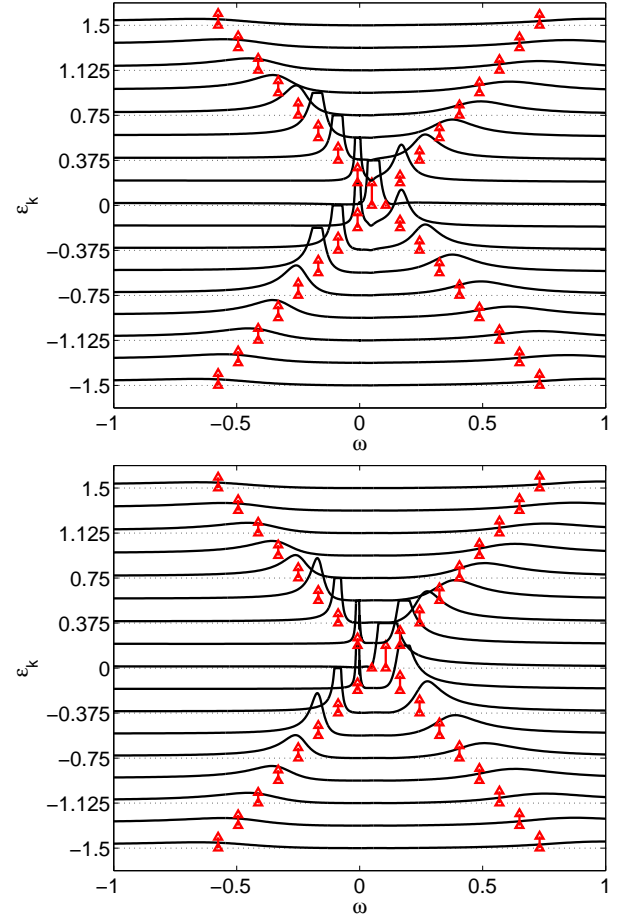


FIG. 12: (Color online) The spectral density $\rho_{\boldsymbol{k},\sigma}(\omega)$ for the spin-up electrons (upper panel) and spin-down (lower panel) plotted as a function of $\omega$ and a sequence of values of $\varepsilon_{\boldsymbol{k}}$ for $U = 3$ and 12.5% doping. Also shown with arrows are the positions of the free quasiparticle excitations, with the height of the arrow indicating the corresponding weight.

$\varepsilon_{\boldsymbol{k}}$. This is most marked in the region near the Fermi level for the spin-up electrons where most of the spectral weight is in the lower band and it is much reduced in the upper band, whereas the opposite is the case for the spin-down electrons. This is reflected in the analytic form of the weights $u_\pm^\sigma(\varepsilon_{\boldsymbol{k}})$, equation (39). For instance, $u_-^\uparrow(\varepsilon_{\boldsymbol{k}})$ corresponding to the lower band $E_{\boldsymbol{k},-}^0$ becomes maximal near the Fermi energy, whereas $u_+^\uparrow(\varepsilon_{\boldsymbol{k}})$ goes to zero there. The finite width of the quasiparticle peaks in $\rho_{\boldsymbol{k},\sigma}(\omega)$ can be described by a RPT, when we take into account the renormalized self-energy $\tilde\Sigma_\sigma(\omega)$ in equation (37). If we, for instance, use the the second order approximation in $\tilde U$, which was illustrated in the last section (31), we get a similar behavior for small $\omega$ as seen for $\rho_{\boldsymbol{k},\sigma}(\omega)$ in figure 12.

From the positions of the peaks in the $\rho_{\boldsymbol{k},\sigma}(\omega)$ spectra we can deduce two branches of an effective dispersion $E_{\boldsymbol{k},\pm}$ for single particle excitations and compare it with the ones for the free quasiparticles $E_{\boldsymbol{k},\pm}^0$. We give the
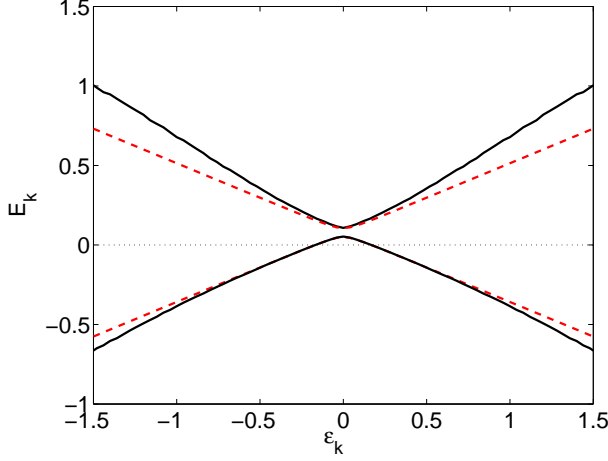
results for $U = 3$ in figure 13.



FIG. 13: (Color online) A plot of the peaks in the spectral density $\rho_{\boldsymbol{k},\sigma}(\omega)$ (full line) as a function of $\varepsilon_{\boldsymbol{k}}$ for $U = 3$ and 12.5% doping compared with the free quasiparticle dispersion $E_{\boldsymbol{k}}^0$ (dashed line).

It can be seen that $E_{\boldsymbol{k},-}^0$ tracks the peak in the lower band closely over a wide range of $\varepsilon_{\boldsymbol{k}}$, $-1.5 < \varepsilon_{\boldsymbol{k}} < 1.5$ (note the bandwidth $W = 4$). This is not the case in the upper band, where $E_{\boldsymbol{k},+}^0$ tracks the peak closely only in the lowest section that lies closest to the Fermi level. As one can see from the dotted line the Fermi level lies in the lower band and intersects the lower band twice. This corresponds to the two values with opposite sign $\varepsilon_{\boldsymbol{k}_{\mathrm{F}}}^{\pm}$ as can be see from equation (34).

The corresponding results for $\boldsymbol{k}$ resolved spectra for $U = 6$ and also 12.5% doping are shown in figure 14.

In order to compare well with the case $U = 3$ we have chosen an identical range for $\omega$ and $\varepsilon_{\boldsymbol{k}}$, although the large spectral peaks near the energy are very close together in this presentation. It can be seen that the overall features are very similar to those seen for $U = 3$. For the spin up spectrum (upper panel) the peaks for the lower band have most of the weight near the Fermi energy, whereas the upper band is suppressed there, and vice versa for the opposite spin direction. The lower bands are tracked well by the free quasiparticles, and we can see that the bands for the larger value of $U$ are significantly flatter. This is also clearly visible in the following figure 15, where we again compare the quasiparticle band with the peak position of the full spectra. On the range shown the lower band $E_{\boldsymbol{k},-}$ completely coincides with the free quasiparticle band $E_{\boldsymbol{k},-}^0$.

From the $\boldsymbol{k}$-resolved spectra in figures 12 and 14 we can also extract the width of the quasiparticle peak $\Delta_{\mathrm{qp}}$ in the spectral density $\rho_{\boldsymbol{k},\sigma}(\omega)$. Its inverse $1/\Delta_{\mathrm{qp}}$ gives a measure of the quasiparticle lifetime. The results for $\Delta_{\mathrm{qp}}$ for the lower band $E_{\boldsymbol{k},-}$ for the two cases $U = 3, 6$ and 12.5% doping are shown in figure 16 as function of $\varepsilon_{\boldsymbol{k}}$. This plot brings out more clearly the feature that can be seen already in figures 12 and 14 (upper panel) that
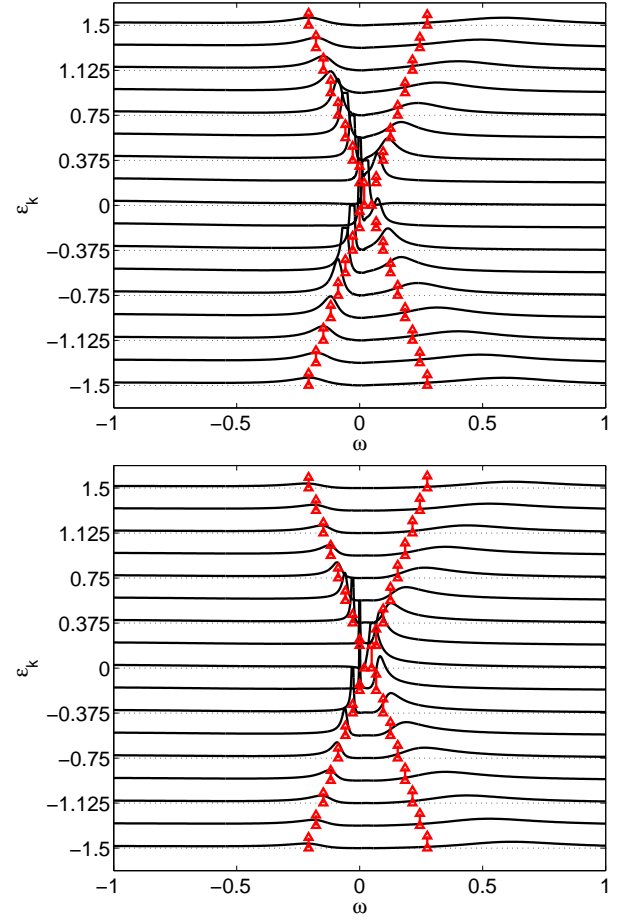


FIG. 14: (Color online) The spectral density $\rho_{\boldsymbol{k},\sigma}(\omega)$ for the spin-up electrons (upper panel) and spin-down (lower panel) plotted as a function of $\omega$ and a sequence of values of $\varepsilon_{\boldsymbol{k}}$ for $U = 6$ and 12.5% doping. Also shown with arrows are the positions of the free quasiparticle excitations, with the height of the arrow indicating the corresponding weight.

the width increases sharply when we move away from the Fermi level and the values for the width $\Delta_{\mathrm{qp}}$ for $U = 6$ are significantly smaller than those for $U = 3$. This is in line with the fact that the local quasiparticle interaction $\tilde{U}$ is smaller for the larger value of the bare interaction $U$ as commented on earlier. The free quasiparticle picture is therefore even more appropriate in the case with stronger interaction. To numerical accuracy the width vanishes at $\varepsilon_{\boldsymbol{k}_{\mathrm{F}}}^{\pm}$ and is finite for the interval $\varepsilon_{\boldsymbol{k}_{\mathrm{F}}}^{-} < \varepsilon_{\boldsymbol{k}} < \varepsilon_{\boldsymbol{k}_{\mathrm{F}}}^{+}$ which lies within the lower band but above the Fermi level.

Another quasiparticle property can be extracted by calculating the derivative with respect to $\varepsilon_{\boldsymbol{k}}$ in equation (19)

$$\frac{\partial E_{\boldsymbol{k},\pm}^0}{\partial \varepsilon_{\boldsymbol{k}}} = \pm \frac{z_\uparrow z_\downarrow \varepsilon_{\boldsymbol{k}}}{\sqrt{\Delta\tilde{\mu}^2 + \tilde{\varepsilon}_{\boldsymbol{k}}^2}}. \tag{42}$$

This gives the value for the curvature $\Delta\tilde{\mu}/z_\uparrow z_\downarrow$ for the regime $\varepsilon_{\boldsymbol{k}} \ll \Delta\tilde{\mu}$, which fits the upper and lower bands in this region. In the regime $|\varepsilon_{\boldsymbol{k}}| \gg \Delta\tilde{\mu}$ $E_{\boldsymbol{k},\pm}^0 \sim \pm\varepsilon_{\boldsymbol{k}}$ so we
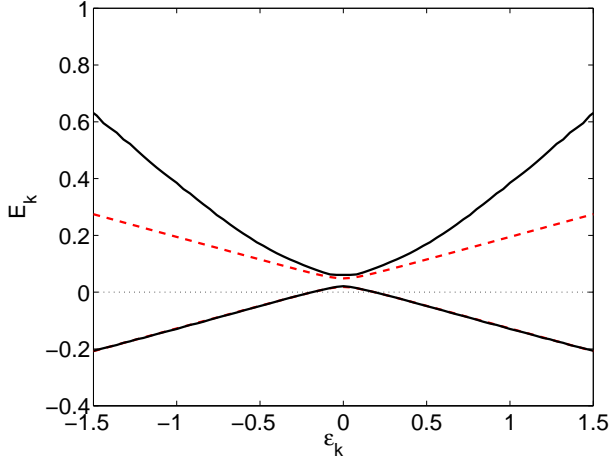
FIG. 15: (Color online) A plot of the peaks in the spectral density $\rho_{\boldsymbol{k},\sigma}(\omega)$ (full line) as a function of $\varepsilon_{\boldsymbol{k}}$ for $U = 6$ and 12.5% doping compared with the free quasiparticle dispersion $E_{\boldsymbol{k}}^0$ (dashed line). On the range shown the lower band $E_{\boldsymbol{k},-}$ completely coincides with the free quasiparticle band $E_{\boldsymbol{k},-}^0$.
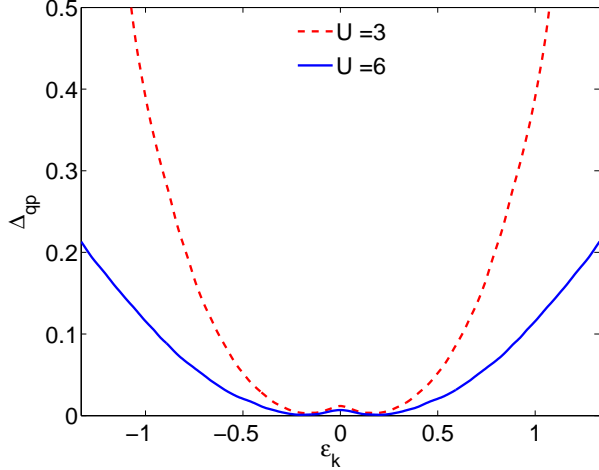


FIG. 16: (Color online) A plot of the width of the peaks $\Delta_{\mathrm{qp}}$ in the spectral density $\rho_{\boldsymbol{k},\sigma}(\omega)$ as a function of $\varepsilon_{\boldsymbol{k}}$ for $U = 3$ (dashed line) and $U = 6$ (full line) and 12.5% doping.

can extract $1/\sqrt{z_\uparrow z_\downarrow}$ as an enhancement of the effective mass $m^*$. The general trend for $m^*/m = 1/\sqrt{z_\uparrow z_\downarrow}$ as function of $U$ can be seen in figure 17 for the case of 12.5% doping.

The fact that the lower band for $U = 6$ seen in figure 15 is flatter than in the case $U = 3$ in figure 13 can be clearly attributed to the smaller value of $\sqrt{z_\uparrow z_\downarrow}$ and larger effective mass. We find a similar behavior of $m^*/m$ as function of $U$ for smaller dopings than shown in figure 17.

With the values for $z_\sigma$ from figures 5 and 6 it can be shown that the effective mass tends to decrease as the doping is reduced. This is in contrast to the behavior of the effective mass in the paramagnetic state which increases as the doping is reduced. As a conse-
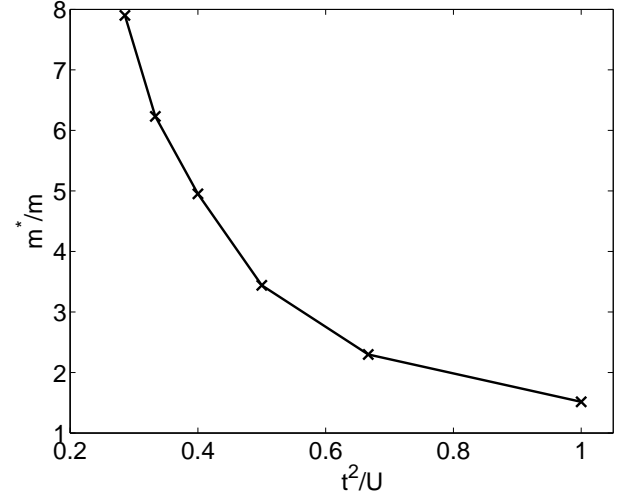


FIG. 17: (Color online) The ratio $m^*/m$ plotted over a range of $t^2/U$ for 12.5% doping.

quence, the antiferromagnetic ordering leads to less pronounced renormalization effects for the effective mass. For large doping the solutions with and without symmetry breaking become more similar and values of the effective masses tend towards the same value.

## V. CONCLUSIONS

We have studied the field induced and spontaneous antiferromagnetic ordering in the hole doped Hubbard model with DMFT-NRG calculations at $T = 0$. A phase diagram separating antiferromagnetic and paramagnetic solutions for different values of doping and interactions $U$ ranging from zero to about 1.5 times the band width $W$ has been established and is in agreement with earlier results by Zitzler et al.[10]. Our main objective has been to analyze the properties of the quasiparticle excitations in the metallic antiferromagnetic state. We presented two different ways of calculating the parameters $z_\sigma$ and $\tilde\mu_{0,\sigma}$, which define the renormalized quasiparticles, and the two sets of results have been shown to be in agreement. We have also been able to deduce the effective on-site quasiparticle interaction $\tilde U$ from the NRG low lying excitations. The low energy properties of the local spectral function can be understood in terms of the free quasiparticle picture. We have used the second order perturbation expansion in powers of $\tilde U$ to estimate the spectral weight in the pseudo-gap region above the Fermi level.

We have been able to compare the position of the peaks found in the $\boldsymbol{k}$-dependent spectral functions with the dispersion relation for the free quasiparticles. The free quasiparticle dispersion gives a very good fit to the position of these peaks in the lower band which intersects the Fermi level. The quasiparticle lifetime, as deduced from the widths of the peaks in the spectrum, increases

for stronger interactions. This is consistent with the fact that the on-site quasiparticle interaction $\tilde{U}$, which gives the quasiparticles a finite lifetime, decreases with increase of $U$ in the same range.

We have found that Luttinger's theorem for the total electron density in the antiferromagnetically ordered state holds within the numerical accuracy for the range of dopings and interactions studied. This is a further indication that many aspects of Fermi liquid description may hold in situations with symmetry breaking.

It is not easy to make a direct comparison of our results with earlier work[3] analyzing the quasiparticle excitations in an metallic antiferromagnet as these have been mainly based on the $t-J$-model for one or two holes in a finite cluster. However, at a semiquantitative level, the overall trend in our results seems to be similar to the results surveyed by Dagotto, where the effective quasiparticle bandwidth $W_{\text{eff}}$ is found to decrease with decreasing $J$.

This is line with our results if we identify $W_{\text{eff}} \sim \sqrt{z_\uparrow z_\downarrow}$ and $J \sim t^2/U$ (see figure 17). Also our values for the wavefunction renormalization $z_\sigma$ are qualitatively similar to those presented in the review article by Dagotto (see fig 27[3]).

## Acknowledgment

[1] P. W. Anderson, Science **235**, 1196 (1987).

[2] P. A. Lee, N. Nagaosa, and X.-G. Wen, Rev. Mod. Phys. **78**, 17 (2006).

[3] E. Dagotto, Rev. Mod. Phys. **66**, 763 (1994).

[4] A.-M. S. Tremblay, B. Kyung, and D. Senechal, Low Temperature Physics **32**, 424 (2006).

[5] W. Metzner and D. Vollhardt, Phys. Rev. Lett. **62**, 324 (1989).

[6] E. Müller-Hartmann, Z. Phys. B **74**, 507 (1989).

[7] R. Bulla, T. Costi, and T. Pruschke (2007), cond-mat/0701105.

[8] J. Bauer and A. C. Hewson (2006), cond-mat/06012161.

[9] A. C. Hewson, Phys. Rev. Lett. **70**, 4007 (1993).

[10] R. Zitzler, T. Pruschke, and R. Bulla, Eur. Phys. J. B **27**, 473 (2002).

[11] J. Hubbard, Proc. R. Soc. London, Ser. A **276**, 238 (1963).

[12] A. Georges, G. Kotliar, W. Krauth, and M. Rozenberg, Rev. Mod. Phys. **68**, 13 (1996).

[13] P. W. Anderson, Phys. Rev. **124**, 41 (1961).

[14] R. Bulla, Phys. Rev. Lett. **83**, 136 (1999).

[15] R. Peters, T. Pruschke, and F. B. Anders, Phys. Rev. B **74**, 245114 (2006).

[16] A. Weichselbaum and J. von Delft (2006), cond-mat/0607497.

[17] F. B. Anders and A. Schiller, Phys. Rev. Lett. **95**, 196801 (2005).

[18] R. Bulla, A. C. Hewson, and T. Pruschke, J. Phys.: Cond. Mat. **10**, 8365 (1998).

[19] V. J. Emery, S. A. Kivelson, and H. Q. Lin, Phys. Rev. Lett. **64**, 475 (1990).

[20] P. G. J. van Dongen, Phys. Rev. Lett. **74**, 182 (1995).

[21] H. J. Schulz, Phys. Rev. Lett. **64**, 1445 (1990).

[22] J. K. Freericks and M. Jarrell, Phys. Rev. Lett. **74**, 186 (1995).

[23] V. J. Emery, S. A. Kivelson, and J. M. Tranquada, Proc. Natl. Acad. Sci. (USA) **96**, 8814 (1999).

[24] B. I. Shraiman and E. D. Siggia, Phys. Rev. Lett. **62**, 1564 (1989).

[25] A. C. Hewson, A. Oguri, and D. Meyer, Eur. Phys. J. B **40**, 177 (2004).

[26] H. R. Krishna-murthy, J. W. Wilkins, and K. G. Wilson, Phys. Rev. B **21**, 1003 (1980).

[27] L. H. Ryder, *Quantum Field Theory* (Cambridge University Press, Cambridge, 1996).

[28] A. C. Hewson, J. Phys.: Cond. Mat. **13**, 10011 (2001).